Research Square

Preprints are preliminary reports that have not undergone peer review.
They should not be considered conclusive, used to inform clinical practice,
or referenced by the media as validated information.

Acidic ZnCl 2 /ZnBr 2 Molten Salt Hydrates for Cellulose Deconstruction and Selective Conversion to 5- Hydroxymethylfurfural

Wenkang Xiao
South China University of Technology
Shihua Yao
South China University of Technology
Yiyuan Zeng
South China University of Technology
Tao Ruan
South China University of Technology
Xinping Ouyang
ceouyang@scut.edu.cn
South China University of Technology

Research Article

Keywords: catalytic conversion of cellulose, biomass derived platform chemicals, metal chloride catalytic system, cellulose decrystallization, furan derivatives, biomass valorization

Posted Date: November 11th, 2026

DOI: https://doi.org/10.21203/rs.3.rs-10782432/v1

License: This work is licensed under a Creative Commons Attribution 4.0 International License.
Read Full License

Additional Declarations: No competing interests reported.

Acidic $ZnCl_2/ZnBr_2$ Molten Salt Hydrates for Cellulose Deconstruction and Selective Conversion to 5-Hydroxymethylfurfural

*Wenkang Xiao, Shihua Yao, Yiyuan Zeng, Tao Ruan, Xinping Ouyang**

**Corresponding author: ceouyang@scut.edu.cn*

School of Chemistry & Chemical Engineering, South China University of Technology, Guangzhou 510640, PR China

Abstract

The single-vessel conversion of cellulose into 5-hydroxymethylfurfural (HMF) provides an efficient route for valorizing lignocellulosic biomass. In this study, an acidic $ZnCl_2/ZnBr_2$ molten salt hydrate (AMSH) system was developed for the two-stage conversion of microcrystalline cellulose (MCC) into HMF. Low-temperature pretreatment effectively disrupted the intra- and intermolecular hydrogen-bonding network of cellulose, reducing its crystalline order. The combined Brønsted and Lewis acidity of the mixed molten salt system facilitated cellulose depolymerization and subsequent HMF formation. Systematically tuning the $ZnBr_2$ fraction concurrently optimized zinc coordination, medium acidity, and the solvation environment; moderate $ZnBr_2$ fractions enhanced cellulose deconstruction and HMF selectivity, whereas excessive $ZnBr_2$ fractions promoted HMF rehydration to levulinic acid. The response surface model predicted a maximum HMF yield of 60.69% at 162.8 °C, 150 min, 2.63 wt% HCl, and 10.35 mol% $ZnBr_2$. DFT calculations indicated that local mixed-halide Zn coordination reduced the calculated electronic energy barrier of the representative 1,2-hydride-transfer step by 40.6 $kJ \cdot mol^{-1}$. These results delineate clear composition–structure–performance relationships for halide-regulated cellulose deconstruction and selective conversion in zinc-based molten salt hydrates.

Keywords: acidic molten salt hydrates; cellulose; 5-hydroxymethylfurfural; halide regulation; Brønsted/Lewis acid

Introduction

With the continued depletion of fossil resources and growing environmental concerns, the high-value utilization of lignocellulosic biomass has become an important research direction for the production of sustainable chemicals and fuels (Liao et al. 2020). 5-Hydroxymethylfurfural (HMF), which contains a furan ring, a hydroxymethyl group, and an aldehyde group, can be further converted into polyester monomers, liquid fuels, and various fine chemicals, making it an important platform chemical (Van Putten et al. 2013; Kong et al. 2020; Jiang et al. 2023). Cellulose consists of glucose units linked by β-1,4-glycosidic bonds and is widely distributed in plant cell walls and agricultural residues. Therefore, the production of HMF from cellulose is consistent with current trends in lignocellulosic biorefining (Yao et al. 2022).

The dense intra- and intermolecular hydrogen-bonding network of cellulose gives rise to a highly ordered crystalline structure, which limits its dissolution in water and most organic solvents and restricts the accessibility of glycosidic bonds to catalytic sites (Medronho et al. 2012; Etale et al. 2023). The conversion of cellulose into HMF typically involves consecutive steps, including glycosidic bond hydrolysis, glucose isomerization, and fructose dehydration. Brønsted acids primarily promote glycosidic bond hydrolysis and fructose dehydration, whereas Lewis acids facilitate glucose ring opening and isomerization (Choudhary et al. 2013; Zhao et al. 2018). Meanwhile, HMF readily undergoes rehydration in acidic aqueous media to form levulinic acid and formic acid, or undergoes condensation reactions to produce humin-like by-products, thereby decreasing HMF selectivity and yield. Therefore, enhancing cellulose reactivity and accessibility, balancing Brønsted and Lewis acid functions, and suppressing secondary HMF reactions are essential for improving the HMF yield (Shi et al. 2022).

Carbon-based solid acids and other multifunctional solid acid catalysts typically operate through a bifunctional mechanism, in which surface Brønsted acid sites, such as sulfonic, carboxyl, and phosphate groups, catalyze glycosidic bond hydrolysis and fructose dehydration, whereas Lewis acid centers derived from supported metal species, metal oxides, or defect sites facilitate glucose ring opening and isomerization (Rezayan et al. 2022; Shi et al. 2024; Yang et al. 2025). Cui et al. (2023) prepared bifunctional carbon-based solid acids from waste bio-tar. By constructing distinct acid sites on a porous carbon framework, they achieved a glucose conversion of 96.1% and an HMF yield of 74.6% under optimal conditions, demonstrating that the coordinated action of dual acid sites can effectively promote the tandem isomerization-dehydration of glucose. Xing et al. (2022) developed bifunctional Hf-β zeolites with Brønsted and Lewis acid sites for cellulose conversion in an H_2O(NaCl)-THF biphasic system, achieving 86.3% conversion and 53.4% HMF yield at 200 °C for 4 h. These findings indicate that acid-site type, acid strength, pore architecture, and surface properties collectively determine HMF selectivity. However, the direct conversion of highly crystalline cellulose remains limited by its poor solubility and the restricted accessibility of glycosidic bonds to active sites.

To simplify the process and enable the one-pot conversion of cellulose into HMF, solid acids have recently been coupled with reaction media capable of activating the cellulose structure. Liu et al. (2025) combined a solid acid with a molten salt hydrate (MSH), in which the molten salt disrupted the hydrogen-bonding network of cellulose and increased the accessibility of crystalline regions, while the solid acid sites catalyzed hydrolysis and subsequent dehydration, thereby promoting the tandem conversion of cellulose into HMF. An HMF yield of 66.88% was obtained at

180 °C after 20 min. However, this system relied on a high LiBr-to-cellulose mass ratio and required an additional Sn-β catalyst and volatile acetone, thereby increasing the complexity of catalyst separation, solvent recovery, and pressurized operation.

Certain acidic ionic liquids (AILs) and deep eutectic solvents (DESs) exhibit a strong ability to dissolve or swell cellulose and can simultaneously serve as reaction media, catalysts, and cocatalysts (Chen et al. 2022). Li et al. (2018) coupled a sulfonated polyphenylene sulfide solid acid (SPPS) with 1-ethyl-3-methylimidazolium bromide ([EMIM]Br), obtaining an HMF yield of 87.2% from glucose, whereas direct cellulose conversion afforded an HMF yield of 68.2%. Xing et al. (2025) developed an FA/LiCl/H_2O DES system that simultaneously served as a cellulose-dissolving medium, a Brønsted acid catalyst for hydrolysis/dehydration, and a Lewis acid modulator. When coupled with a DMSO conversion stage, this system afforded an HMF yield of 61.4% at 180 °C after 20 min. Coupling cellulose structural activation with subsequent catalytic conversion in acidic DESs can effectively alleviate solid–liquid mass transfer limitations; however, existing ionic liquids and DESs generally suffer from high viscosity, limited heat and mass transfer, high solvent loading, and difficulties in HMF recovery.

HMF production from glucose often affords high yields, whereas substantially lower yields are generally obtained when cellulose is used as the feedstock. This difference is primarily attributed to the crystalline structure of cellulose, which restricts its dissolution and hydrolysis, thereby necessitating relatively high Brønsted acidity. However, excessive Brønsted acidity accelerates HMF rehydration and condensation, disrupts the balance between Brønsted and Lewis acid functions, and suppresses Lewis acid-catalyzed glucose isomerization. High Brønsted acid concentrations also promote the conversion of HMF into levulinic acid and other by-products. Inorganic MSHs can disrupt the hydrogen-bonding network of cellulose (Sen et al. 2013; Rodriguez Quiroz et al. 2019; Wang et al. 2025). Previous studies have demonstrated that acidified LiBr, LiCl, and $ZnCl_2$ molten salt hydrate systems facilitate cellulose hydrolysis, whereas Lewis-acidic Zn and Al halides promote cellulose conversion into HMF. Nevertheless, single molten salt systems often fail to simultaneously meet the requirements for cellulose dissolution and HMF production (Deng et al. 2015; Li et al. 2016; Liu et al. 2022; Wei et al. 2023). In pure $ZnCl_2$ hydrate, moderate Lewis acidity limits glucose isomerization, whereas in pure $ZnBr_2$ hydrate, higher apparent proton activity accelerates the parasitic rehydration of HMF to levulinic acid. Furthermore, introducing a polar aprotic co-solvent such as DMSO can effectively suppress HMF rehydration by modifying the local solvation shell.

Based on this rationale, a mixed $ZnCl_2$/$ZnBr_2$ acidic molten salt hydrate (AMSH) system was developed for the one-pot, two-stage conversion of microcrystalline cellulose into HMF. To elucidate the structural deconstruction of cellulose, the treated solids were recovered through water-induced precipitation for comprehensive characterization of pretreatment-induced structural changes (XRD, ATR-FTIR, solid-state ^{13}C CP/MAS NMR, XPS, TGA, and SEM). In a separate conversion route, catalytic HMF production was performed via low-temperature pretreatment followed by in situ DMSO addition. By systematically adjusting the composition of the $ZnBr_2$ hydrate system, a viable molten salt strategy is established to simultaneously optimize zinc coordination, medium acidity, and water content, thereby effectively controlling cellulose depolymerization and achieving high-yield formation of HMF. This study provides a comprehensive understanding of the composition-structure-property relationships in halogen-regulated cellulose conversion within zinc-based molten salt hydrates.

Materials and Methods

Materials

Microcrystalline cellulose (MCC), glucose (99%), HMF (99%), hydrochloric acid (HCl, 37%), phosphoric acid (H_3PO_4, ≥85 wt.% in H_2O), anhydrous zinc chloride ($ZnCl_2$), anhydrous zinc bromide ($ZnBr_2$), dimethyl sulfoxide (DMSO), D-(+)-cellobiose (98%), ethyl acetate (EtOAc), isopropanol (i-PrOH), n-butanol (n-BuOH), and trimethylphosphine oxide (TMPO) were purchased from Aladdin Industrial Corporation (Shanghai, China). All chemicals were used as received without further purification.

Preparation of AMSH

Individual $ZnCl_2$-AMSH and $ZnBr_2$-AMSH were prepared by separately mixing anhydrous $ZnCl_2$ or $ZnBr_2$ with deionized water at a salt-to-water molar ratio of 1:3, followed by the addition of 0-4 wt% HCl, calculated as the mass of pure HCl relative to the total mass of AMSH. The mixtures were stirred until homogeneous solutions were obtained.

Dissolution Pretreatment of Cellulose

For structural characterization, a larger scale experiment was performed. In a typical procedure, 1 g of MCC was added to a beaker containing 10 g of AMSH, and the mixture was heated at 80 °C under mechanical stirring at 500 rpm for 10 min. Excess deionized water was then added, and the precipitate was collected by centrifugation. The regenerated cellulose was thoroughly washed with deionized water to remove residual salts and subsequently freeze-dried to obtain molten-salt-treated cellulose for structural characterization.

Characterization of Cellulose

The structural characteristics and crystalline order of cellulose before and after mixed molten salt treatment were examined by X-ray diffraction (XRD; D8 Advance) using Cu Kα radiation (λ = 0.154059 nm) at 40 kV and 30 mA over a 2θ range of 5°-60° at a scanning rate of 0.01° s^{-1}. Functional groups were analyzed by attenuated total reflectance Fourier-transform infrared spectroscopy (ATR-FTIR; Nicolet iS50). Solid-state 13C cross-polarization/magic-angle-spinning nuclear magnetic resonance (^{13}C CP/MAS NMR) spectra were recorded on a Bruker spectrometer (Ascend 600 MHz magnet and AVANCE NEO console, Bruker, Switzerland) equipped with a 4 mm dual-resonance HX high-temperature probe. Surface elemental composition and chemical states were investigated by X-ray photoelectron spectroscopy (XPS; K-Alpha+), with binding energies calibrated against the C 1s peak at 284.8 eV. Thermal stability was evaluated using a thermogravimetric analyzer (TG 209 F3). Sample morphology was observed by field-emission scanning electron microscopy (SEM; Hitachi SU8200) at an accelerating voltage of 5-10 kV. Particle-size distributions were measured using a laser particle-size analyzer, and the volume-weighted mean diameter D(4,3) was reported.

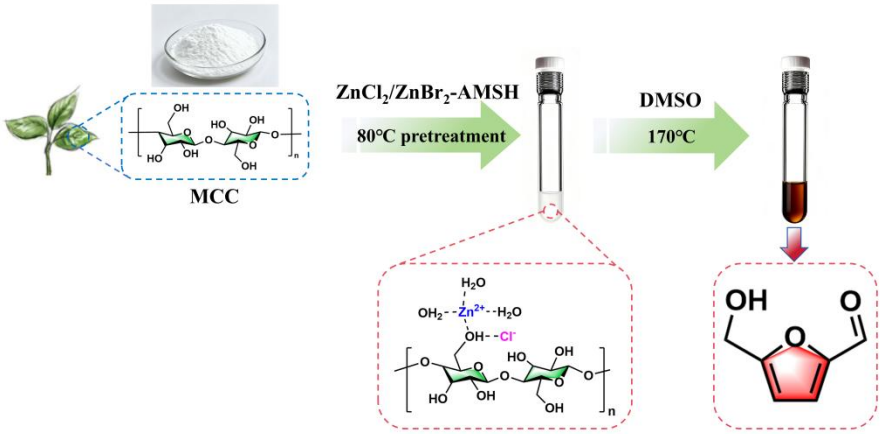
NMR Measurements

Acidity was characterized using the TMPO-based ^{31}P NMR method. Solution-state ^{31}P NMR spectra were recorded on a Bruker AVANCE III HD 600 MHz NMR spectrometer equipped with a 5 mm dual-broadband probe. TMPO was used as a ^{31}P NMR probe to characterize the relative Lewis acid response of the molten salt hydrates. Deuterated molten salt hydrates with different $ZnBr_2$ molar fractions were prepared by replacing H_2O with D_2O while maintaining $n(D_2O)/n(Zn) = 3$. For

AMSH samples containing 2 wt% HCl, the acid was added as an aqueous solution, and the introduced H_2O was included in the total water content. A 0.50 mL aliquot of the molten salt sample was mixed with 0.055 mmol TMPO. After the mixture was stirred to homogeneity, cooled to 298 K, and equilibrated, it was transferred to an NMR tube for spectral acquisition. The TMPO/D_2O system was used as the free-probe reference. Identical acquisition and processing parameters were used for all samples.

Cellulose Conversion

In a typical run, 0.1 g of MCC and 1 g of AMSH were charged into a 38 mL thick-walled pressure-resistant vessel. The mixture was pretreated at 80 °C for 10 min, after which 3 mL of DMSO was added. The reaction was then conducted under continuous stirring at the specified temperature for 90-150 min in an oil bath. After the reaction, the vessel was rapidly quenched in an ice-water bath. The reaction mixture was subsequently diluted with deionized water, and the supernatant was collected by centrifugation for HPLC analysis. Dissolution and conversion of cellulose in the AMSH system was demonstrated in Scheme 1.



Scheme 1. Dissolution and conversion of cellulose in the AMSH system

Product Analysis

The supernatant was filtered through a 0.22 μm polyethersulfone (PES) membrane to remove particulate impurities. HMF was quantified by high-performance liquid chromatography (HPLC; Shimadzu LC-2030C) using a ZORBAX StableBond C18 column (5 μm, 4.6 × 250 mm) and a UV detector set at 280 nm. The column temperature was maintained at 35 °C, and the mobile phase consisted of an aqueous phosphoric acid solution (0.1% H_3PO_4) and methanol at a volume ratio of 95:5, with a flow rate of 0.8 mL min^{-1}. Glucose, fructose, and levulinic acid were quantified using an Agilent 1260 Infinity II liquid chromatograph equipped with a Bio-Rad HPX-87H column, a refractive-index detector (RID-G7162A), and an autosampler with an adjustable injection volume of 1-100 μL. The mobile phase was a 50 mmol L^{-1} aqueous H_2SO_4 solution; the injection volume was 5 μL, the column temperature was 50 °C, and the flow rate was 0.5 mL min^{-1}. Quantification was performed using the external-standard method, and calibration curves were constructed for HMF, glucose, and levulinic acid. The calibration curves were shown in Figs. S5-S7. Cellulose conversion and product yields were calculated as follows:

$$\text{Cellulose conversion(wt\%)} = \left(1 - \frac{\text{mass of MCC remaining}}{\text{mass of MCC added}}\right) \times 100 \quad (1)$$

188 Glucose yield：$Y_{Glu}(\%)=\left(\frac{C_{Glu}\times MW_{MCC}(162)}{C_{MCC}\times MW_{Glu}(180)}\right)\times 100$ （2）

189 HMF yield：$Y_{HMF}(\%)=\left(\frac{C_{HMF}\times MW_{MCC}(162)}{C_{MCC}\times MW_{HMF}(126)}\right)\times 100$ （3）

190 Levulinic acid yield：$Y_{LA}(\%)=\left(\frac{C_{LA}\times MW_{MCC}(162)}{C_{MCC}\times MW_{LA}(116)}\right)\times 100$ （4）

191 **Density Functional Theory Calculations**

192 All density functional theory (DFT) calculations were performed using the Gaussian 16
193 package. A simplified mixed-halide Zn coordination model containing one Zn center coordinated
194 with Cl and Br ligands (denoted as the ZnClBr model) was constructed to represent a plausible local
195 coordination environment under conditions where Cl^- and Br^- coexist. The geometries of glucose,
196 the glucose-ZnClBr complex, fructose, and the corresponding transition-state (TS) structures were
197 optimized at the M06-2X/6-311G(d,p) level of theory. Solvent effects were accounted for using the
198 integral equation formalism polarizable continuum model (IEF-PCM) with dimethyl sulfoxide
199 (DMSO) as the solvent.

200 To compare changes in the reactivity of different atomic sites in glucose upon local
201 coordination with the mixed-halide Zn species, Fukui-function analysis based on conceptual density
202 functional theory (CDFT) was performed using the Multiwfn program. Orbital-weighted condensed
203 Fukui functions were calculated from the electron-density distributions of the neutral (N), anionic
204 (N+1), and cationic (N-1) states. The electrophilic Fukui index (f^+) characterizes the electron-
205 accepting ability of an atom, whereas the nucleophilic Fukui index (f^-) describes its electron-
206 donating ability, thereby evaluating the electronic response of each active site during the reaction.
207 Transition-state structures were optimized using the Berny algorithm with the
208 Opt=(TS,CalcFC,NoEigenTest) keyword. All stationary points were subsequently characterized by
209 vibrational-frequency analysis. A structure was identified as a transition state when it exhibited a
210 single imaginary frequency associated with the proton and hydride transfers involved in glucose
211 isomerization. The activation energy was calculated as the electronic-energy difference between the
212 optimized reactant and transition state.
213

Results and discussion

Dissolution and structural changes of cellulose during AMSH treatment

To distinguish the effect of low-temperature AMSH pretreatment on MCC structure from the subsequent HMF formation process, MCC was first treated with AMSH systems containing varying $ZnBr_2$ molar contents at 80 °C for 10 min, followed by sample regeneration through water addition. The recovered samples were subsequently subjected to multiple complementary characterization techniques to evaluate changes in crystalline structure, chemical environment, thermal behavior, and particle size (Fig. 1).

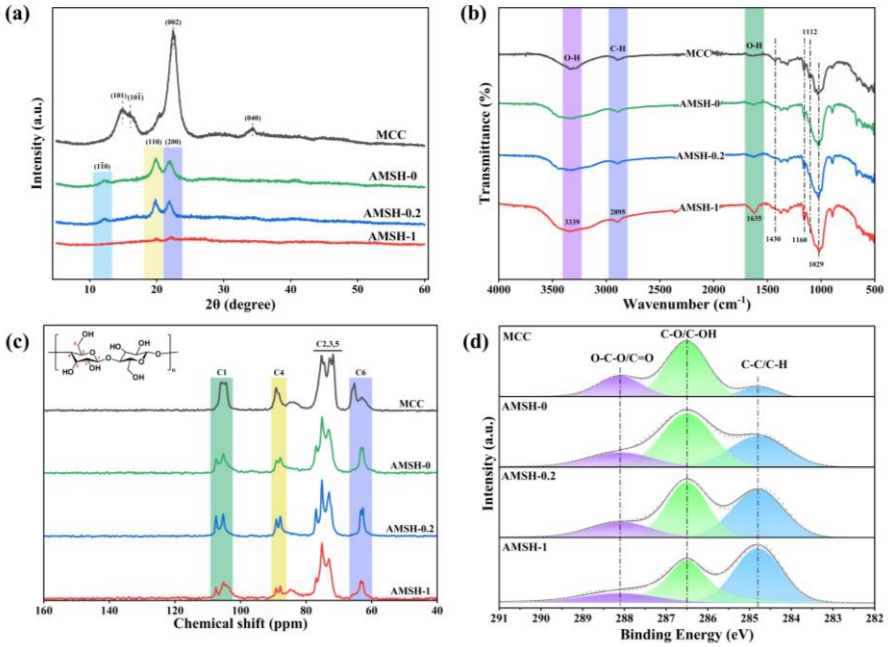


Fig. 1 Structural characterization of MCC before and after AMSH treatment: (a) XRD patterns; (b) FTIR spectra; (c) ^{13}C CP/MAS NMR spectra; (d) high-resolution C 1s XPS spectra (MCC denotes microcrystalline cellulose; AMSH-0, AMSH-0.2, and AMSH-1 denote cellulose samples obtained after pretreatment with molten salt hydrates containing different $ZnBr_2$ molar fractions at 80 °C for 10 min)

As shown in Fig. 1a, pristine MCC exhibited characteristic diffraction peaks of cellulose I at 2θ = 14.8°, 16.3°, 22.5°, and 34.5°. After AMSH treatment, diffraction signals associated with cellulose II appeared at 2θ = 12.2°, 20.0°, and 21.9°, indicating that the acidified molten salt disrupted the original ordered crystalline packing and induced a transition from cellulose I to cellulose II with lower crystalline order (French 2014; Li et al. 2021). Among the treated samples, the cellulose treated with AMSH-1 exhibited the weakest and broadest XRD diffraction peaks, indicating the most pronounced reduction in crystalline order.

The FTIR spectra (Fig. 1b) showed that both pristine and molten-salt-treated cellulose retained characteristic bands at 3339 cm^{-1} (O-H stretching), 2895 cm^{-1} (C-H stretching), 1160 cm^{-1} (C-O-C stretching of β-1,4-glycosidic linkages), and 1029 cm^{-1} (C-O vibration), indicating that the acidified molten salt treatment did not substantially degrade the cellulose backbone (Arnata et al. 2020; Wang et al. 2023; Xing et al. 2025). Compared with MCC, the bands at 1430 and 1112 cm^{-1} were weakened in the treated samples, with the 1430 cm^{-1} band attributed to the CH_2 symmetric bending (scissoring) vibration, a crystallinity-sensitive mode of cellulose I. These FTIR changes are consistent with the reduced crystalline order of cellulose I and corroborate the XRD evidence in Fig. 1a.

The CP/MAS ^{13}C NMR spectra of cellulose before and after molten salt treatment are shown in Fig. 1c. For pristine MCC, the C1 signal of the anhydroglucose units appeared at 102-108 ppm, whereas the crystalline and amorphous C4 signals were observed at 89 and 84 ppm, respectively. The overlapping C2, C3, and C5 signals were detected in the 70-78 ppm region, and the crystalline and amorphous C6 signals were identified at 65 and 62 ppm, respectively (Kono et al. 2004; Idström et al. 2016). After AMSH treatment, the main C1-C6 skeletal signals were retained, indicating that no substantial chemical derivatization occurred during pretreatment. However, the sharp C1 signal of MCC became noticeably broadened. The crystalline C4 signal at 89 ppm decreased in intensity, while the C6 signal shifted from the crystalline component at 65 ppm toward the amorphous component at 62 ppm, indicating disruption of the original hydrogen-bonding network in MCC. After the introduction of 20 mol% $ZnBr_2$, the relative profile of the overlapping C2/C3/C5 region in AMSH-0.2 treated cellulose changed, indicating that the mixed $ZnCl_2/ZnBr_2$ molten salt further altered the hydrogen-bonding environment around the anhydroglucose units and facilitated the formation of local cellulose II structures. In contrast, the C1, C4, and C6 signals of AMSH-1 treated cellulose were markedly broadened and exhibited lower resolution; the disordered C4 component near 84 ppm and the less ordered C6 component at 62-63 ppm were relatively enhanced. These changes indicated that pure $ZnBr_2$ molten salt caused the most pronounced disruption of interchain hydrogen bonds and local crystalline order. Overall, the results showed that $ZnCl_2/ZnBr_2$ acidified molten salt treatment promoted the transformation of cellulose into a less ordered structure while preserving the cellulose molecular backbone.

The C 1s XPS spectra (Fig. 1d) showed changes in the relative proportions of the C-C/C-H (284.8 eV), C-O/C-OH (286.5 eV), and O-C-O (288.1 eV) components (Wang et al. 2026). The C-O/C-OH component is primarily derived from C2-C6 of the anhydroglucose units, whereas the O-C-O component corresponds mainly to C1, which is bonded to both the ring oxygen and the glycosidic oxygen. After AMSH treatment, the fitted C-C/C-H contribution increased in all treated cellulose samples, indicating a redistribution of the surface carbon environments. These changes were consistent with the reduced crystallinity observed by XRD, the reconstruction of O-H hydrogen bonds indicated by FTIR, and the attenuation of crystalline C4/C6 signals in the solid-state NMR spectra. Together, these results indicate that the $ZnCl_2/ZnBr_2$ acidified molten salt primarily enhances cellulose accessibility by modifying its surface chemical environment and hydrogen-bonding structure.

TGA was used to evaluate the changes in the thermal stability of cellulose after AMSH treatment (Fig. S1). Pristine MCC remained thermally stable below 310 °C, and its primary thermal decomposition occurred at 320-360 °C, with a maximum DTG mass-loss peak at 335 °C. In contrast, cellulose treated with AMSH-0, AMSH-0.2, or AMSH-1 exhibited lower initial degradation temperatures. AMSH-0 and AMSH-0.2 treated cellulose began to show pronounced mass loss at 180-220 °C, whereas AMSH-1 treated cellulose displayed a broader continuous mass loss region, indicating markedly reduced thermal stability after regeneration. The lower degradation temperatures and broader DTG peaks are associated with decreases in cellulose crystallinity and degree of polymerization (Phanthong et al. 2016), indicating that $ZnCl_2/ZnBr_2$ acidified molten salt treatment disrupted the original hydrogen-bonding network and ordered crystalline structure of cellulose (Burger et al. 2020).

Changes in cellulose particle size before and after treatment were examined by laser particle size analysis. As shown in Fig. S2, the volume-weighted mean diameter D(4,3) of pristine MCC

was 41.46 μm. After treatment with AMSH-0, AMSH-0.2, and AMSH-1, the mean particle sizes decreased to 18.05, 15.08, and 12.32 μm, respectively, indicating cellulose particle fragmentation and deconstruction (Kim et al. 2023).Overall, Fig. 1 shows that AMSH treatment reduced the crystalline order, thermal stability, and particle size of cellulose while retaining its principal molecular backbone.

SEM images obtained before and after molten salt treatment (Fig. 2) revealed that pristine MCC exhibited a sheet-like or short rod-like morphology with relatively dense and smooth particle surfaces, indicating intact crystalline packing. Upon acidified molten salt treatment, the cellulose transformed into a loose, delaminated, and irregularly fragmented morphology, demonstrating that the acidified molten salt disrupted the crystalline structure of cellulose. As the $ZnBr_2$ molar content increased, the regenerated cellulose displayed an increasing tendency toward fragmentation and pore formation. In particular, the sample (d) exhibited more pronounced flocculent fragments and a loose structure, suggesting that elevated $ZnBr_2$ content promoted the loss of crystalline order in cellulose.

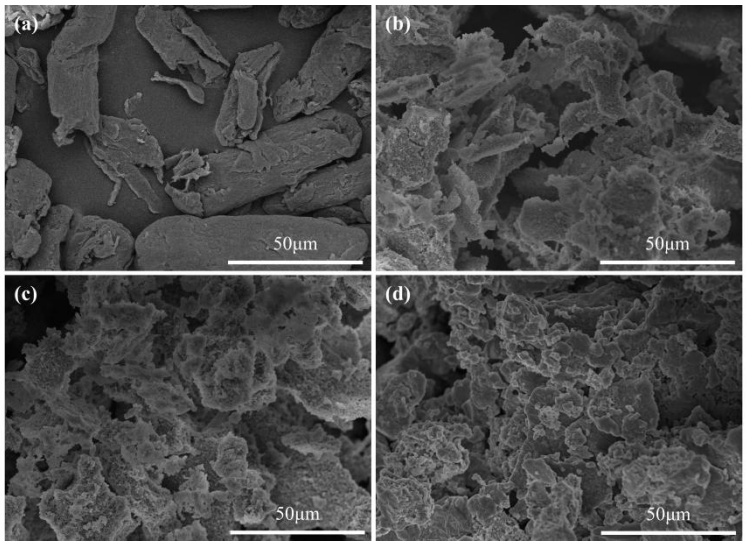


Fig. 2 SEM images of MCC samples: (a) MCC; (b) MCC after AMSH-0 treatment; (c) MCC after AMSH-0.2 treatment; (d) MCC after AMSH-1 treatment

In summary, acidified molten salt pretreatment effectively disrupts the hydrogen-bonding network of cellulose molecules. The dissolution of cellulose in AMSH could be attributed to the coordination interactions between Zn^{2+} species and the oxygen atoms of cellulose hydroxyl groups, as well as hydrogen-bonding/ion-dipole interactions between Cl^-/Br^- ions and the hydrogen atoms of cellulose hydroxyls (Leipner et al. 2000; Brendler et al. 2001; Sen et al. 2013). The coordination of metal ions with hydroxyl groups may weaken hydration interactions from the inner coordination sphere of metal-water complexes; these ion-cellulose interactions effectively disrupt the hydrogen bonds connecting cellulose chains (Deng et al. 2015; Sadula et al. 2017), transforming MCC from highly crystalline cellulose I into low-crystallinity cellulose II. The retention of C1-C6 skeletal signals indicates that the anhydroglucose structural units remain essentially intact during this process. With increasing $ZnBr_2$ content, the extents of decrystallization, morphological fragmentation, and thermal degradation were markedly enhanced, suggesting that Br^- incorporation enhanced the ability of the acidified molten salt system to disrupt cellulose structure. The proposed dissolution mechanism of cellulose in AMSH is illustrated in Fig. 3.

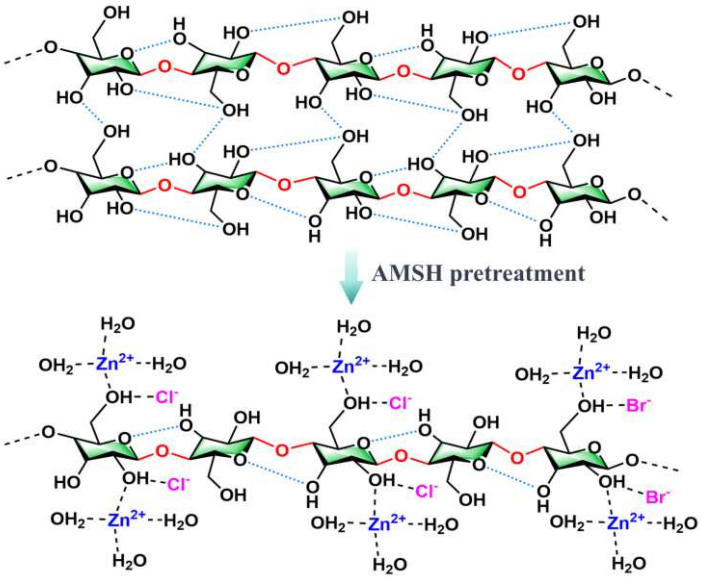


Fig. 3 Proposed mechanism for cellulose dissolution in the AMSH

Acidity of the AMSH Media

The intrinsic acidity of the solvent medium is another crucial factor governing glycosidic bond hydrolysis, glucose isomerization, and fructose dehydration. Accordingly, the apparent pH of the AMSH medium was determined upon 10-fold dilution, and the acid strength response was characterized by ^{31}P NMR spectroscopy using the TMPO probe; the results are shown in Fig. 4.

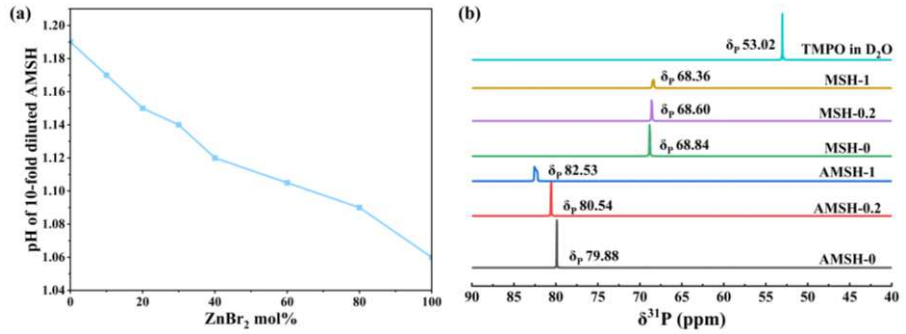


Fig. 4 Acidity characterization of zinc halide molten salt hydrate systems with varying $ZnBr_2$ molar contents: (a) apparent pH of AMSH systems upon 10-fold dilution; (b) ^{31}P NMR spectra of TMPO probe in MSH and AMSH systems containing 2 wt% HCl. In MSH-x and AMSH-x, x denotes the molar content of $ZnBr_2$ relative to total zinc halides; the HCl mass fraction in AMSH was fixed at 2 wt%

As shown in Fig. 4a, the apparent pH of the tenfold-diluted AMSH samples gradually decreased as the $ZnBr_2$ molar fraction increased, indicating increased apparent proton activity and stronger Brønsted acidity. The TMPO-^{31}P NMR results in Fig. 4b showed only minor variations in chemical shift among the MSH samples without HCl. After the addition of 2 wt% HCl, all signals shifted markedly downfield, and the magnitude of the shift increased with the $ZnBr_2$ molar fraction. AMSH-1 exhibited the most downfield chemical shift, indicating that it afforded the strongest TMPO-^{31}P probe response among the investigated AMSH samples under the aforementioned HCl-containing conditions.

In concentrated salt solutions, $ZnCl_2$ typically forms $[ZnCl_x(H_2O)_{6-x}]$ coordination complexes. After the addition of 2 wt% HCl, a substantial amount of Cl^- enters the Zn coordination sphere, displaces coordinated water molecules, and may form $[ZnCl_4]^{2-}$ complexes. Because of the high

electronegativity of Cl^-, the Lewis acidity of Zn^{2+} is relatively low, which hinders the isomerization of glucose generated by hydrolysis. In contrast, owing to the larger ionic radius of Br^-, $ZnBr_2$ complexes are thermodynamically more likely to form dinuclear $[Zn_2Br_6]^{2-}$ species or fully hydrated octahedral $[Zn(H_2O)_6]^{2+}$ species (Dhakal et al. 2023). Consequently, the introduction of $ZnBr_2$ may alter the Zn-based coordination environment and enhance the Lewis acid characteristics of the system, while hydrolysis-derived Brønsted acidity is also increased, thereby contributing to improved HMF formation. However, the stronger acidic environment in $ZnBr_2$-AMSH facilitated the further rehydration of HMF to LA, which resulted in a relatively low HMF yield. Therefore, the synergistic integration of both AMSH systems is required to enhance HMF selectivity.

Effects of Reaction Medium Composition and Process Parameters on Cellulose to HMF Conversion

After the structural deconstruction ability and acidic characteristics of the AMSH medium were clarified, the effect of component variables on the product distribution of cellulose catalytic conversion to HMF was further investigated (Fig. 5).

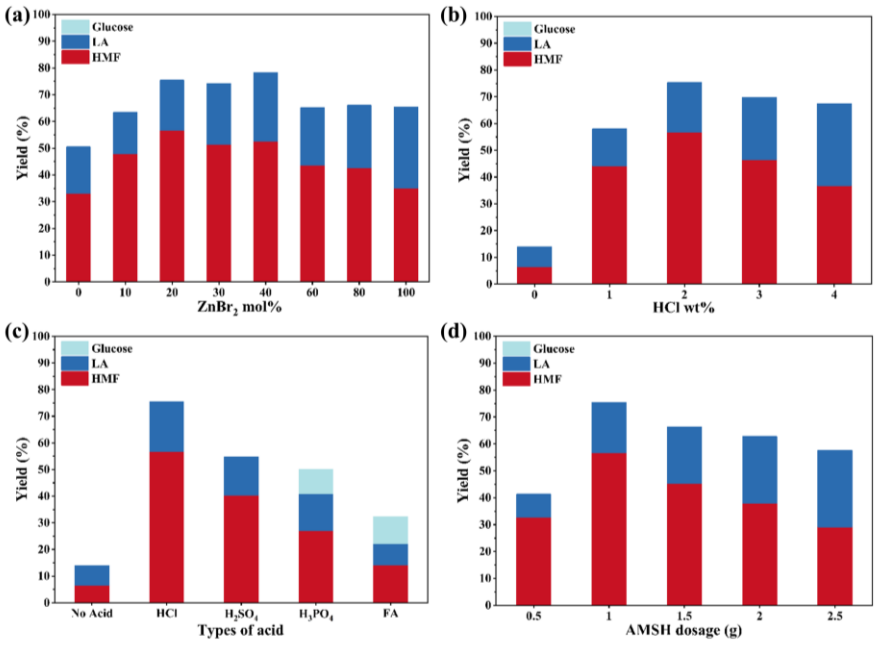


Fig. 5 Effects of AMSH composition and acidic environment on the product distribution from cellulose conversion: (a) $ZnBr_2$ molar fraction relative to total zinc salts; (b) HCl mass fraction; (c) acid type; (d) AMSH dosage. Unless otherwise stated, the reaction conditions were as follows: MCC, 0.1 g; AMSH, 1.0 g; $ZnBr_2$, 20 mol%; HCl, 2 wt%; pretreatment at 80 °C for 10 min; DMSO, 3 mL; and reaction at 170 °C for 120 min. In the acid-type experiments, all acids were added at the same mass fraction

As shown in Fig. 5a, the HMF yield in the pure $ZnCl_2$-AMSH was 33.16%. With the increase $ZnBr_2$ molar fraction, the HMF yield first increased, reaching a maximum of 56.76% at 20 mol%, and then gradually decreased. In the pure $ZnBr_2$-AMSH system, the HMF yield dropped to 35.13%, while the yield of levulinic acid (LA) significantly increased to 30.17%. Combined with the characterization results above, the disruption of the crystalline structure of cellulose by $ZnCl_2$-AMSH is relatively limited (Fig. 1), which restricts substrate accessibility to the active sites during the subsequent hydrolysis and conversion processes, thus resulting in a low HMF yield. In contrast, although $ZnBr_2$-AMSH can more effectively disrupt the cellulose crystalline structure and exhibit stronger dissolution capacity, this system possesses a lower apparent pH and higher apparent proton

activity (Fig. 4a). This elevated protonic acidity markedly accelerates the parasitic secondary rehydration of HMF into LA (Olivito et al. 2023; Rodriguez Quiroz et al. 2023), thereby leading to the decline in the final HMF yield. Therefore, introducing an optimal $ZnBr_2$ mole fraction (20 mol%) achieves the best trade-off among cellulose structure decrystallization/activation, catalytic conversion activity, and the inhibition of HMF over-degradation.

As shown in Fig. 5b, when no HCl was added (0 wt%), the HMF yield was only 6.2% (with an LA yield of 7.7%). Although the unacidified MSH can promote the decrystallization and swelling of cellulose, its inherent proton acidity is insufficient to effectively cleave the β-1,4-glycosidic bonds. This is consistent with the fact that the unacidified MSH sample in Fig. 4b lacks the characteristic downfield shift (>80 ppm) caused by protonation. Upon introducing 1 wt% HCl, the HMF yield increased sharply to 43.8% and reached a maximum of 56.76% at 2 wt% HCl loading, indicating that sufficient Brønsted acidity is critical to driving cellulose depolymerization, hydrolysis, and subsequent sugar dehydration. However, when the HCl dosage was further increased to 4 wt%, the HMF yield decreased to 36.7%, whereas the LA yield soared to 30.9%. This indicates that excessive Brønsted acidity accelerates the secondary side reactions, including the rehydration of HMF to LA and its cross-condensation into humins (Rodriguez Quiroz et al. 2023; Jong et al. 2025).

As shown in Fig. 5c, the acid type had a significant effect on the product distribution. Compared with H_2SO_4, H_3PO_4, and formic acid, the system with HCl added achieved the highest HMF yield (56.76%). In the systems with H_3PO_4 and formic acid, a substantial amount of unconverted glucose (~9–10%) remained in the reaction solution, indicating that their weak acidity was insufficient to drive complete conversion. In contrast, although complete glucose consumption was achieved in the H_2SO_4 system, the resulting HMF yield (40.2%) was lower than that of the HCl system. The above results show that HCl provides the most effective Brønsted acid sites, which synergize with the molten salt hydrates medium to disrupt intermolecular hydrogen bonds and decrystallize cellulose (Wang et al. 2025), thereby effectively promoting the cascade conversion of cellulose to HMF.

As shown in Fig. 5d, the HMF yield was low at low AMSH dosages because the available molten salt and active acid sites were insufficient to disrupt the cellulose hydrogen-bonding network and catalyze hydrolysis. Increasing the AMSH dosage enhanced cellulose deconstruction and sugar conversion, leading to a marked increase in HMF yield. Upon a further increase in AMSH dosage, the HMF yield decreased while the LA yield increased. This change may be attributed to the concurrent increases in system acidity and water content, which promoted the further conversion of HMF into LA.

The effects of process parameters on the product distribution during cellulose conversion were investigated, as shown in Fig. 6.

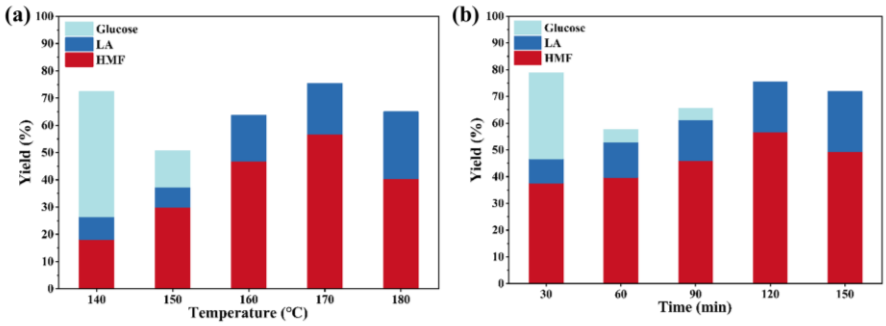


Fig. 6 Effects of the two-stage process parameters on the product distribution during cellulose conversion: (a) reaction temperature (120 min); (b) reaction time (170 °C). Unless otherwise stated, the reaction conditions were as follows: MCC 0.1 g, AMSH 1.0 g, $ZnBr_2$ 20 mol%, HCl 2 wt%, pretreatment at 80 °C for 10 min, DMSO 3 mL, and reaction at 170 °C for 120 min

As shown in Fig. 6a and Fig. 6b, reaction temperature and time markedly affected the product distribution during cellulose conversion. At lower temperatures or shorter reaction times, a considerable amount of glucose remained in the system, indicating that the glucose generated by cellulose hydrolysis had not undergone sufficient isomerization and dehydration. As the temperature and reaction time increased, the amount of residual glucose gradually decreased and the HMF yield increased, reaching 56.76% at 170 °C after 120 min. When the temperature was further increased to 180 °C or the reaction time was extended to 150 min, the HMF yield decreased to 40.50% and 49.33%, respectively, while the LA yield increased. These results suggest that excessively high temperatures and prolonged reaction times promote HMF rehydration and condensation, thereby decreasing HMF selectivity (Wu et al. 2023; Rezayan et al. 2023).

As shown in Fig. S3, the co-solvent type also markedly affected the product distribution. DMSO has high polarity and hydrogen-bond basicity and can alter the local solvent arrangement around fructose isomers (Li et al. 2023), thereby favoring pathways leading to HMF formation. DMSO also reduces the effective water concentration near HMF and consequently suppresses its rehydration into LA. The water-only system afforded a low HMF yield (~8.5%) and high LA yield (~22.5%) despite complete glucose consumption, indicating that a single aqueous phase is unfavorable for HMF stabilization against rehydration. In contrast, in GVL, a considerable amount of unreacted glucose (~16.5%) remained alongside a low HMF yield (~5.8%) and elevated LA yield (~25.0%). The lower HMF yields obtained with isopropanol (~37.5%) and n-butanol (~32.0%) may be attributed to poorer compatibility and less efficient mass transfer between the alcohol solvents and the concentrated molten salt phase. These results indicate that the co-solvent affects not only HMF stability but also the competition among cellulose hydrolysis, glucose conversion, and side reactions. Therefore, DMSO is more suitable as a co-solvent for the second-stage conversion in the acidified molten salt hydrates system.

As shown in Fig. S4, the DMSO dosage markedly affected HMF selectivity. At low DMSO dosages, the relatively high water content in the acidified molten salt phase rendered HMF more susceptible to rehydration, resulting in a higher LA yield. When the DMSO dosage was increased to 3 mL, the HMF yield reached its maximum(56.76%). As a highly polar aprotic solvent, DMSO stabilizes the intermediates involved in glucose isomerization and fructose dehydration and preferentially solvates HMF, thereby reducing its tendency to undergo rehydration (Jin et al. 2021). Further increasing the DMSO dosage decreased the HMF yield. With fixed AMSH and HCl dosages, excessive DMSO reduces the effective concentrations of Zn halide and protonic acid species per unit volume. In addition, the lower relative water content and water activity may cause glycosidic-bond hydrolysis to become rate-limiting. Previous studies have demonstrated that solvent composition and Cl^- collectively alter the glucose conversion pathway and the free energy distribution of intermediates; therefore, either excessively high or excessively low organic solvent fractions are unfavorable for the tandem hydrolysis-isomerization-dehydration process (Sanpitakseree et al. 2022).

RSM-Based Optimization of Process Parameters

Because the conversion of cellulose into HMF involves multiple sequential steps, including cellulose crystalline deconstruction, glycosidic-bond hydrolysis, isomerization to fructose, and

dehydration, the process parameters may exhibit interaction effects. Therefore, the Box-Behnken design (BBD) was employed to systematically investigate the effects of reaction temperature (A), reaction time (B), HCl mass fraction (C), and $ZnBr_2$ molar fraction (D) on the HMF yield. The factor levels were selected based on preliminary single-factor experiments, with three coded levels (-1, 0, +1) summarized in Table S1. A total of 27 experimental runs with three center-point replicates were performed in a randomized order to minimize the likelihood of systematic experimental bias. Table S2 presents the experimental design matrix along with the experimental and predicted HMF yields. Multiple regression analysis of the experimental data yielded the following second-order polynomial equation in terms of coded values:

$$\text{HMF yield} = 55.89 - 4.83 \times A + 2.84 \times B + 0.99 \times C - 2.43 \times D + 0.6675 \times AB - 9.95 \times AC + 0.58 \times AD + 2.12 \times BC - 2.69 \times BD - 6.83 \times CD - 7.63 \times A^2 - 2.97 \times B^2 - 13.45 \times C^2 - 5.08 \times D^2$$

The statistical significance of the regression model was assessed by analysis of variance (ANOVA) using the F-test, and the results are presented in Table S3. The R^2 value of the model was 0.9661, indicating a good fit of the regression equation and satisfactory predictive capability within the investigated design space. The model F-value of 24.45 ($p < 0.0001$) confirms that the regression model is statistically highly significant. Specifically, within the investigated factor ranges, reaction temperature (A), reaction time (B), and $ZnBr_2$ molar fraction (D) all exerted highly significant linear effects on the HMF yield ($p < 0.01$). Although the linear term of HCl dosage (C) had a p-value of 0.1963, its quadratic term (C^2, $F = 153.60$, $p < 0.0001$) and interaction terms (AC, $p < 0.0001$; CD, $p = 0.0001$) were highly significant, demonstrating that the acid loading primarily governs HMF selectivity through strong nonlinear and synergistic interactions with reaction temperature and salt composition. The lack-of-fit F-value was 2.60 ($p = 0.3097 > 0.05$), which confirms that no significant lack of fit was detected and validates the adequacy of the model.

Based on the comprehensive analysis above, the following conclusions can be drawn: reaction temperature, reaction time, and $ZnBr_2$ molar content all exerted highly significant effects on the HMF yield. Accordingly, these three factors were selected as interactive independent variables, with HMF yield as the dependent variable, and response surface plots were constructed based on the quadratic polynomial model to further elucidate the effects of the main factors and their interactions on the HMF yield, as shown in Fig. 7.

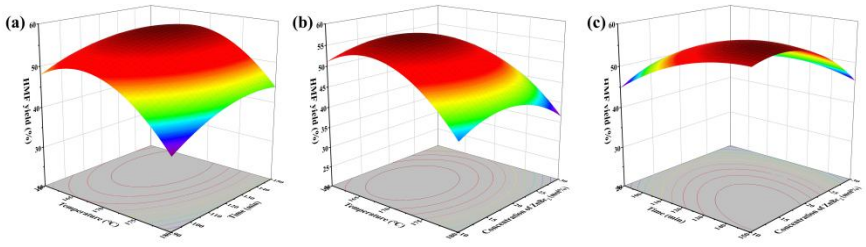


Fig. 7 Three-dimensional response surface plots showing the interactive effects of reaction factors on HMF yield: (a) reaction temperature and reaction time; (b) reaction temperature and $ZnBr_2$ molar content; (c) reaction time and $ZnBr_2$ molar content

The RSM results revealed that the optimal conditions for the conversion of cellulose into HMF were a reaction temperature of 162.8 °C, a reaction time of 150 min, a $ZnBr_2$ molar content of 10.35 mol%, and an HCl mass fraction of 2.63 wt%. Under the optimal conditions predicted by the model within the investigated factor ranges, the model predicted a maximum HMF yield of 60.69%.

Effect of Mixed-Halide Zn Coordination on the Elementary Steps of Glucose Isomerization

The aforementioned experimental results demonstrated that the appropriate introduction of $ZnBr_2$ can modulate the Cl^-/Br^- composition and the local coordination environment around the Zn center, thereby influencing sugar intermediate conversion and HMF selectivity. To preliminarily examine the role of mixed-halide Zn coordination in the glucose isomerization process at the molecular level, the 1,2-hydride transfer elementary step, a representative pathway in Lewis acid-catalyzed glucose isomerization reported by Kim et al. (2020), was selected for DFT calculations. Considering that various hydrated and halide-coordinated species may coexist in the actual $ZnCl_2/ZnBr_2$ molten salt, a simplified local coordination model containing one Zn center coordinated with Cl and Br ligands was constructed, and compared with the non-Zn-coordinated pathway. The effects of mixed-halide Zn coordination on the electronic structure of glucose and the isomerization process were investigated through orbital-weighted (OW) Fukui function analysis, transition-state searching, and reaction barrier calculations.

The isomerization of glucose to fructose essentially involves carbonyl migration during the aldose-to-ketose transformation. Kim et al. proposed that after glucose undergoes ring opening to form a linear intermediate, it can proceed through a 1,2-hydride-transfer followed by ring closure to afford fructose, wherein the hydride transfer represents an important kinetically controlling step in the metal chloride-catalyzed systems investigated(Kim et al. 2020). The mechanism is illustrated in Fig. 8. Glucose first undergoes ring-opening to form a linear intermediate bearing an aldehyde group at C1, followed by a 1,2-hydride transfer from C2 to C1 concomitant with a proton transfer from O2 to O1. During this process, the C2-H bond is gradually cleaved and a new C1-H bond is formed; meanwhile, the C1=O1 carbonyl is converted into a C1-O1 hydroxyl group, whereas the C2-O2 single bond is transformed into a C2=O2 carbonyl group. Consequently, the carbonyl position migrates from C1 to C2, accomplishing the transformation from an aldose to a ketose skeleton.

In this process, the C1 aldehyde group, the C2 hydroxyl group, and the intervening C1-C2 region constitute the key reactive center of the isomerization. The carbonyl oxygen O1 participates in electron redistribution and carbonyl polarization, playing a critical role in stabilizing the transition-state structure and facilitating the hydride transfer. Therefore, the coordination position of the Lewis acidic Zn center with glucose depends not only on the electron-donating ability of the oxygen atoms but also on its capacity to modulate the electronic structure of the key reactive region and stabilize the transition state. In the absence of Zn coordination, the aforementioned hydride transfer, proton transfer, and carbonyl reconstruction rely predominantly on the substrate itself, and the charge redistribution in the transition state is not adequately stabilized, thus requiring the surmounting of a higher energy barrier. Upon introduction of the simplified mixed-halide Zn model, the Zn center coordinates with the oxygen-containing sites of glucose, which can modulate the electronic response of the O1-C1-C2-O2 region and restrict the relative configurations of the relevant atoms, thereby facilitating the C2→C1 hydride transfer and the concomitant proton transfer.

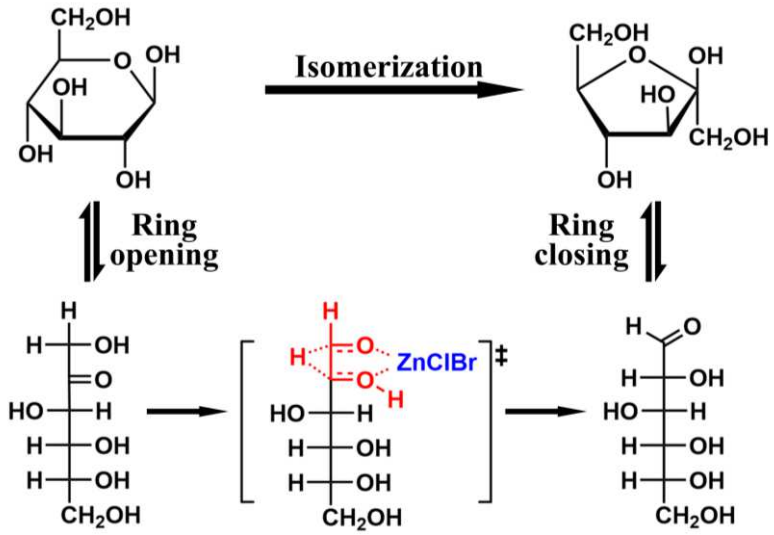


Fig. 8 Representative 1,2-hydride transfer elementary step in the simplified mixed-halide Zn coordination model (Kim et al. 2020)

Mixed-halide Zn local coordination induces pronounced changes in the condensed Fukui functions of the glucose reactive center, as shown in Fig. 9. For the f^+ Fukui function associated with nucleophilic attack, the O1 site exhibits the highest electron-accepting response both before and after coordination; however, its value decreases upon coordination from 0.2704 to 0.1041, indicating that Zn coordination does not merely enhance the electrophilic reactivity of O1 but rather modulates its local electronic response. For f^-, the values for the O1-O6 sites decrease markedly upon Zn coordination, with O1 showing the most significant change (from 0.1041 to 0.0138), demonstrating that the local electron-donating response of the oxygen atoms is suppressed due to their participation in Zn-O coordination. These results indicate that the Zn center in the simplified mixed-halide coordination model alters the response of glucose oxygen-containing sites to electron addition and removal, leading to a redistribution of local reactivity at the reaction center. This redistribution may enhance carbonyl polarization and thereby facilitate the C2→C1 hydride transfer and subsequent carbonyl reconstruction.

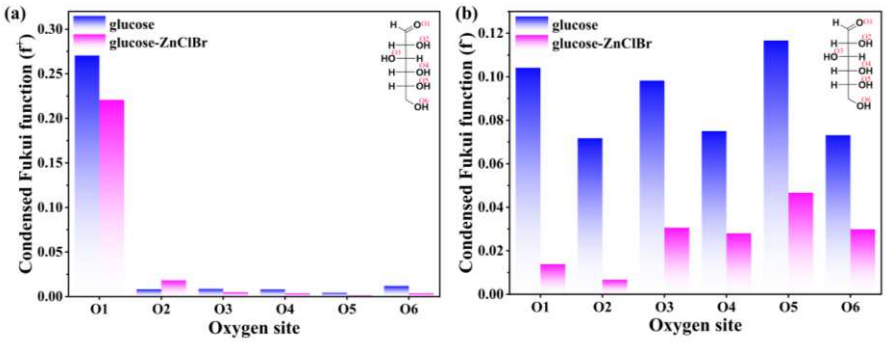


Fig. 9 Comparison of condensed Fukui functions at the O1-O6 sites of glucose before and after ZnClBr model coordination: (a) f^+ (nucleophilic attack); (b) f^- (electrophilic attack)

Fig. 10 illustrates the activation energy profiles for two reaction pathways: Path 1 represents the energy diagram for glucose isomerization to fructose without Zn coordination, and Path 2 represents that with ZnClBr model coordination. To intuitively reflect the effect of local Zn coordination on the hydride transfer step, the initial states of both pathways were shifted to 0 kJ·mol^{-1}. DFT calculations based on the simplified mixed-halide Zn coordination model revealed that the

activation energy for glucose isomerization to fructose was 175.5 kJ·mol^{-1} under non-Zn-coordinated conditions. Upon coordination with the ZnClBr model, the activation energy decreased to 134.9 kJ·mol^{-1}. Compared with the non-Zn-coordinated pathway, the electronic energy barrier for the investigated glucose isomerization hydride transfer step was reduced by 40.6 kJ·mol^{-1}, indicating that the mixed-halide local coordination of the Zn center facilitates sugar intermediate isomerization, suggesting a kinetically more favorable hydride-transfer step.

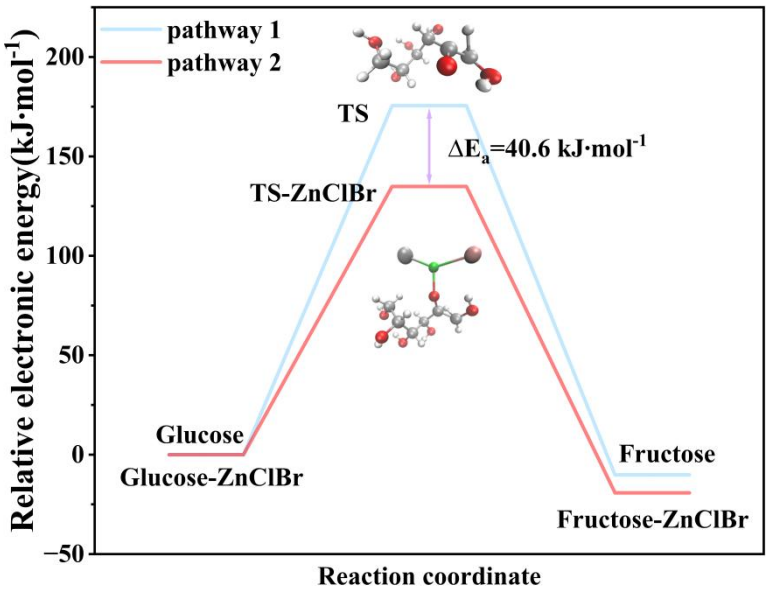


Fig. 10 Energy diagram for the 1,2-hydride transfer step in glucose isomerization with and without the simplified ZnClBr coordination model

Conclusion

The acidified $ZnCl_2$/$ZnBr_2$ mixed molten salt hydrates pretreatment effectively disrupts the intra- and intermolecular hydrogen-bonding network and ordered crystalline structure of MCC, inducing a transition from cellulose I toward cellulose II with reduced crystalline order. In the mixed molten salt medium, an appropriate $ZnBr_2$ molar fraction enhances cellulose deconstruction, improves substrate accessibility, and optimizes HMF selectivity, which is consistent with concurrent changes in the Zn^{2+} coordination environment and medium acidity. However, an excessively high $ZnBr_2$ fraction and elevated Brønsted acidity accelerate secondary HMF rehydration to LA and condensation to humins. Within the range of factors investigated, the response surface model predicted that the maximum HMF yield of MCC conversion was 60.69% under the optimal conditions (162.8 °C, 150 min, 2.63 wt% HCl, and 10.35 mol% $ZnBr_2$). In addition, DFT calculations based on a simplified ZnClBr coordination model indicate that local mixed-halide Zn coordination reduces the electronic energy barrier of the key 1,2-hydride transfer step in glucose isomerization by 40.6 kJ·mol^{-1}. This study demonstrates that acidified $ZnCl_2$/$ZnBr_2$ mixed molten salt hydrates effectively couple cellulose decrystallization with composition-tunable acidity, providing valuable theoretical and practical guidance for the high-value conversion of cellulose into furan platform chemicals.

578

Data availability

The data supporting this study are available when reasonably requested from the corresponding author.

References

Arnata IW, Suprihatin S, Fahma F, et al (2020) Cationic modification of nanocrystalline cellulose from sago fronds. Cellulose 27:3121–3141. https://doi.org/10.1007/s10570-019-02955-3

Brendler E, Fischer S, Leipner H (2001) 7Li NMR as probe for solvent–cellulose interactions in cellulose dissolution. Cellulose 8:283–288. https://doi.org/10.1023/A:1015120107514

Burger D, Winter A, Subbiahdoss G, et al (2020) Partial amorphization of cellulose through zinc chloride treatment: a facile and sustainable pathway to functional cellulose nanofibers with flame-retardant and catalytic properties. ACS Sustain Chem Eng 8:13576–13582. https://doi.org/10.1021/acssuschemeng.0c03492

Chen L, Xiong Y, Qin H, Qi Z (2022) Advances of ionic liquids and deep eutectic solvents in green processes of biomass-derived 5-hydroxymethylfurfural. ChemSusChem 15:e202102635. https://doi.org/10.1002/cssc.202102635

Chen X, Chen X, Cai X-M, et al (2018) Cellulose dissolution in a mixed solvent of tetra(*n* -butyl)ammonium hydroxide/dimethyl sulfoxide via radical reactions. ACS Sustain Chem Eng 6:2898–2904. https://doi.org/10.1021/acssuschemeng.7b04491

Choudhary V, Mushrif SH, Ho C, et al (2013) Insights into the interplay of lewis and brønsted acid catalysts in glucose and fructose conversion to 5-(hydroxymethyl)furfural and levulinic acid in aqueous media. J Am Chem Soc 135:3997–4006. https://doi.org/10.1021/ja3122763

Cui X, Zheng L, Li Q, Guo Y (2023) A remarkable bifunctional carbon-based solid acid catalyst derived from waste bio-tar for efficient synthesis of 5-hydroxymethylfurfural from glucose. Chem Eng J 474:146006. https://doi.org/10.1016/j.cej.2023.146006

Deng W, Kennedy JR, Tsilomelekis G, et al (2015) Cellulose hydrolysis in acidified LiBr molten salt hydrate media. Ind Eng Chem Res 54:5226–5236. https://doi.org/10.1021/acs.iecr.5b00757

Devi B, Arumugam SM, Kumar S, et al (2023) Thermodynamic insights into MgBr2-mediated glucose interconversion to fructose undertaking multiple reaction pathways by applying the macro- and micro-kinetic principles. ACS Sustain Chem Eng 11:3284–3296. https://doi.org/10.1021/acssuschemeng.2c06027

Dhakal D, Driscoll DM, Govind N, et al (2023) The evolution of solvation symmetry and composition in Zn halide aqueous solutions from dilute to extreme concentrations. Phys Chem Chem Phys 25:22651–22661. https://doi.org/10.1039/D3CP01559A

Duffy JA, Ingram MD (1978) Acidic nature of metal aquo complexes: proton-transfer equilibriums in concentrated aqueous media. Inorg Chem 17:2798–2802. https://doi.org/10.1021/ic50188a023

Etale A, Onyianta AJ, Turner SR, Eichhorn SJ (2023) Cellulose: a review of water interactions, applications in composites, and water treatment. Chem Rev 123:2016–2048. https://doi.org/10.1021/acs.chemrev.2c00477

French AD (2014) Idealized powder diffraction patterns for cellulose polymorphs. Cellulose 21:885–896. https://doi.org/10.1007/s10570-013-0030-4

Idström A, Schantz S, Sundberg J, et al (2016) 13C NMR assignments of regenerated cellulose from solid-state 2D NMR spectroscopy. Carbohydr Polym 151:481–487. https://doi.org/10.1016/j.carbpol.2016.05.107

Jiang Z, Zeng Y, Hu D, et al (2023) Chemical transformations of 5-hydroxymethylfurfural into highly added value products: present and future. Green Chem 25:871–892. https://doi.org/10.1039/D2GC03444A

Jin C, Xiang N, Zhu X, et al (2021) Selective 5-hydroxymethylfurfural production from cellulose formate in DMSO-H2O media. Appl Catal B Environ 285:119799. https://doi.org/10.1016/j.apcatb.2020.119799

Jong E de, Mascal M, Constant S, et al (2025) The origin, composition, and applications of industrial humins – a review. Green Chem 27:3136–3166. https://doi.org/10.1039/D4GC06244B

Kim HU, Kim JW, Seo S, Jae J (2023) Hydrolysis of regenerated cellulose from ionic liquids and deep eutectic solvent over sulfonated carbon catalysts. RSC Adv 13:8153–8162. https://doi.org/10.1039/d2ra08224a

Kim Y, Mittal A, Robichaud DJ, et al (2020) Prediction of hydroxymethylfurfural yield in glucose conversion through investigation of lewis acid and organic solvent effects. ACS Catal 10:14707–14721. https://doi.org/10.1021/acscatal.0c04245

Kong Q-S, Li X-L, Xu H-J, Fu Y (2020) Conversion of 5-hydroxymethylfurfural to chemicals: A review of catalytic routes and product applications. Fuel Process Technol 209:106528. https://doi.org/10.1016/j.fuproc.2020.106528

Kono H, Numata Y, Erata T, Takai M (2004) 13C and 1H resonance assignment of mercerized cellulose II by two-dimensional MAS NMR spectroscopies. Macromolecules 37:5311–5316. https://doi.org/10.1021/ma030465k

Leipner H, Fischer S, Brendler E, Voigt W (2000) Structural changes of cellulose dissolved in molten salt hydrates. Macromol Chem Phys 201:2041–2049. https://doi.org/10.1002/1521-3935(20001001)201:15%3C2041::AID-MACP2041%3E3.0.CO;2-E

Li N, Bian H, Zhu JY, et al (2021) Tailorable cellulose II nanocrystals (CNC II) prepared in mildly acidic lithium bromide trihydrate (MALBTH). Green Chem 23:2778–2791. https://doi.org/10.1039/D1GC00145K

Li N, Pan X, Alexander J (2016) A facile and fast method for quantitating lignin in lignocellulosic biomass using acidic lithium bromide trihydrate (ALBTH). Green Chem 18:5367–5376. https://doi.org/10.1039/C6GC01090C

Li R, Lin Q, Liu Y, et al (2023) Insights into solvent effect on selective production of furfural and 5-hydroxymethylfurfural from fructose. J Catal 424:162–172. https://doi.org/10.1016/j.jcat.2023.05.022

Li Z, Su K, Ren J, et al (2018) Direct catalytic conversion of glucose and cellulose. Green Chem 20:863–872. https://doi.org/10.1039/C7GC03318D

Liao Y, Koelewijn S-F, Van Den Bossche G, et al (2020) A sustainable wood biorefinery for low–carbon footprint chemicals production. Science 367:1385–1390. https://doi.org/10.1126/science.aau1567

Liu G, Xie Y, Wei C, et al (2022) Synergistic catalysis of species in molten salt hydrate for conversion of cellulose to 5-hydroxymethylfurfural. Biomass Bioenergy 158:106363.

https://doi.org/10.1016/j.biombioe.2022.106363

Liu H, Lin J, Liu Q, et al (2025) Enhanced production of 5-hydroxymethylfurfural from cellulose via synergistic catalysis of solid acid and molten salt hydrates solvent. ChemSusChem 18:e202402776. https://doi.org/10.1002/cssc.202402776

Medronho B, Romano A, Miguel MG, et al (2012) Rationalizing cellulose (in)solubility: reviewing basic physicochemical aspects and role of hydrophobic interactions. Cellulose 19:581–587. https://doi.org/10.1007/s10570-011-9644-6

Olivito F, Algieri V, Tallarida MA, et al (2023) High-yield synthesis of HMF from glucose and fructose by selective catalysis with water-tolerant rare earth metal triflates assisted by choline chloride. Green Chem 25:1679–1689. https://doi.org/10.1039/D2GC04046H

Phanthong P, Guan G, Ma Y, et al (2016) Effect of ball milling on the production of nanocellulose using mild acid hydrolysis method. J Taiwan Inst Chem Eng 60:617–622. https://doi.org/10.1016/j.jtice.2015.11.001

Rezayan A, Wang K, Nie R, et al (2022) Eco-friendly preparation of phosphated gallia: A tunable dual-acidic catalyst for the efficient 5-hydroxymethylfurfural production from carbohydrates. J Catal 414:186–198. https://doi.org/10.1016/j.jcat.2022.09.004

Rezayan A, Zhang Y, Li B, Xu CC (2023) Catalytic conversion of cellulose to 5-hydroxymethylfurfural: advancements in heterogeneous catalysts and cutting-edge hydrolysis strategies. ChemCatChem 15:e202300973. https://doi.org/10.1002/cctc.202300973

Rodriguez Quiroz N, Chen T-H, Caratzoulas S, Vlachos DG (2023) Direct brønsted acid-catalyzed dehydration of glucose to HMF in methyl isobutyl ketone. ACS Catal 13:14221–14232. https://doi.org/10.1021/acscatal.3c03153

Rodriguez Quiroz N, Padmanathan AMD, Mushrif SH, Vlachos DG (2019) Understanding acidity of molten salt hydrate media for cellulose hydrolysis by combining kinetic studies, electrolyte solution modeling, molecular dynamics simulations, and 13C NMR experiments. ACS Catal 9:10551–10561. https://doi.org/10.1021/acscatal.9b03301

Sadula S, Oesterling O, Nardone A, et al (2017) One-pot integrated processing of biopolymers to furfurals in molten salt hydrate: understanding synergy in acidity. Green Chem 19:3888–3898. https://doi.org/10.1039/C7GC01709J

Sanpitakseree C, Motagamwala AH, Dumesic JA, Neurock M (2022) Solvent and chloride ion effects on the acid-catalyzed conversion of glucose to 5-hydroxymethylfurfural. ACS Sustain Chem Eng 10:8275–8288. https://doi.org/10.1021/acssuschemeng.2c00651

Sen S, Martin JD, Argyropoulos DS (2013) Review of cellulose non-derivatizing solvent interactions with emphasis on activity in inorganic molten salt hydrates. ACS Sustain Chem Eng 1:858–870. https://doi.org/10.1021/sc400085a

Shi N, Zhu Y, Qin B, et al (2022) Conversion of cellulose into 5-hydroxymethylfurfural in an H2O/tetrahydrofuran/cyclohexane biphasic system with Al2(SO4)3 as the catalyst. Cellulose 29:2257–2272. https://doi.org/10.1007/s10570-022-04455-3

Shi X, Xing X, Liu W, et al (2024) Cellulose conversion to 5-hydroxymethylfurfural via a simple and efficient phosphate-doped hafnium oxide catalyst. Renew Energy 226:120425. https://doi.org/10.1016/j.renene.2024.120425

Van Putten R-J, Van Der Waal JC, De Jong E, et al (2013) Hydroxymethylfurfural, A Versatile Platform Chemical Made from Renewable Resources. Chem Rev 113:1499–1597. https://doi.org/10.1021/cr300182k

Wang B, Nie Y, Kang Z, Liu X (2023) Effects of coagulating conditions on the crystallinity, orientation and mechanical properties of regenerated cellulose fibers. Int J Biol Macromol 225:1374–1383. https://doi.org/10.1016/j.ijbiomac.2022.11.195

Wang P, Huang Z, Wu M, et al (2026) Two-second surface-confined reconstruction of cellulose paper via a recyclable molten salt hydrate for water-resistant bioplastics. Green Chem 28:9636–9649. https://doi.org/10.1039/D6GC01239F

Wang X, Li L, Xie X, et al (2025) Fractionation of birch sawdust into carbohydrates and high purity lignin by ZnBr2 molten salt hydrates under mild conditions. Int J Biol Macromol 307:142241. https://doi.org/10.1016/j.ijbiomac.2025.142241

Wei C, Liu G, Xie Y, et al (2023) Cellulose dissolution and conversion into 5-hydroxymethylfurfural in mixed molten salt hydrate. Cellulose 30:801–813. https://doi.org/10.1007/s10570-022-04967-y

Wu H, Zhang R, Zhai Y, et al (2023) Solvent effects enable efficient tandem conversion of cellulose and its monosaccharides towards 5-hydroxymethylfurfural. ChemSusChem 16:e202201809. https://doi.org/10.1002/cssc.202201809

Xing X, Hu R, Liu W, et al (2025) A three-way deep eutectic solvent integrating solubilization-brønsted/lewis acids for efficient 5-hydroxymethylfurfural production from cellulose. Green Chem 27:10823–10836. https://doi.org/10.1039/D5GC03124A

Xing X, Shi X, Hu R, et al (2022) Hf-β zeolites as highly efficient catalysts for the production of 5-hydroxymethylfurfural from cellulose in biphasic system. Int J Biol Macromol 222:3014–3023. https://doi.org/10.1016/j.ijbiomac.2022.10.076

Yang Y, Li Y, Deng L, et al (2025) The critical role of crystal phases of $LaPO_4$ in controlling the acidic sites for the production of 5-hydroxymethylfurfural from glucose. Green Chem 27:10915–10929. https://doi.org/10.1039/D5GC01931A

Yao Y, Chen S, Zhang M (2022) Sustainable approaches to selective conversion of cellulose into 5-hydroxymethylfurfural promoted by heterogeneous acid catalysts: a review. Front Chem 10: https://doi.org/10.3389/fchem.2022.880603

Zhao Y, Wang S, Lin H, et al (2018) Influence of a lewis acid and a brønsted acid on the conversion of microcrystalline cellulose into 5-hydroxymethylfurfural in a single-phase reaction system of water and 1,2-dimethoxyethane. RSC Adv 8:7235–7242. https://doi.org/10.1039/C7RA13387A

Statements and Declarations

Acknowledgements

The authors are thankful for financial supports from the National Key Research and Development Program of China (2024YFB4206002).

Funding

This study was financially supported by the National Key Research and Development Program of China (2024YFB4206002).

Author information

Authors and Affiliations

School of Chemistry and Chemical Engineering, South China University of Technology, 510640, China

Wenkang Xiao, Shihua Yao, Yiyuan Zeng, Tao Ruan, Xinping Ouyang

Contributions

WX: Investigation, Writing–original draft; SY: Density Functional Theory (DFT) Calculations; YZ: Investigation, Data curation; TR: Data curation; XO: Conceptualization, Writing – review & editing.

Corresponding author

Correspondence to Xinping Ouyang

Ethics declarations

Conflict of interests

The authors have no relevant financial or non-financial interests to disclose.

Supplementary Files

This is a list of supplementary files associated with this preprint. Click to download.

- Supplementarymaterial.pdf